Journal of Petroleum Science and Engineering 174 (2019) 984–996

Contents lists available at ScienceDirect

Journal of Petroleum Science and Engineering

journal homepage: www.elsevier.com/locate/petrol

Corrosion inhibition by amitriptyline and amitriptyline based formulations for steels in simulated pickling and acidizing media

Ekemini B. Ituen[a,b], Moses M. Solomon[c], Saviour A. Umoren[c,*], Onyewuchi Akaranta[b]

[a] Materials and Oilfield Chemistry (MOC) Research Group, Department of Chemistry, University of Uyo, Uyo, Nigeria
[b] African Centre of Excellence in Oilfield Chemicals Research, Institute of Petroleum Studies, University of Port Harcourt, Choba, Nigeria
[c] Center for Research Excellence in Corrosion, Research Institute, King Fahd University of Petroleum and Minerals, Dhahran, 31261, Saudi Arabia

ARTICLE INFO

Keywords:
Amitriptyline
Industrial application
Steels
Corrosion inhibitor formulations
Acidic environment
Corrosion inhibition

ABSTRACTS

Investigation into amitriptyline (AMI) as a corrosion inhibitor for different grades of pipeline steels (X80, J55 and mild steel) was undertaken under static conditions in 3.7% and 15% HCl solution and temperature ranging from 30 to 90 °C using electrochemical, gravimetric, and surface screening approaches. AMI is adjudged an effective steel corrosion inhibitor in 3.7% HCl at 30 °C but poor inhibitor at high temperatures and in 15% HCl. The values of enthalpy of adsorption and variation of protection efficacy with temperature point to physical interaction between AMI molecules and the steel surface. Evidence of formation of adsorbed film on the specimen surface has been found via Scanning electron microscope (SEM) and energy dispersive spectroscopy (EDAX) screening. Various formulations consisting of AMI as the base component and other additives (potassium iodide, glutathione and N-acetyl cysteine) have been developed. The formulations were tested at different experimental conditions and inhibition performance compared with that of a commercial corrosion inhibitor. Results obtained show that AMI based formulations can compete favorably with commercial inhibitor even at severe conditions. In 15% HCl solution and temperature of 90 °C, inhibition efficiency of 94% is recorded for commercial inhibitor and 92% for AMI based formulation. AMI based formulation can be utilized as effective corrosion inhibitor in oil and gas production.

1. Introduction

Hydrocarbons can still be recovered from some depleted wells by acidizing or reservoir fracture techniques. This involves passing acid solution down a well bore (usually with force) into the formation rocks to etch it and create larger flow channels (Gandossi, 2013; Blattel and Davidson, 2016). Hydrochloric acid (HCl) is frequently used for this operation because it reacts completely with the formation rocks but it is highly corrosive. Typical concentrations of HCl used is in the range of 5–15% or sometimes 25% depending on whether the formation rock is composed of sandstone or limestone (Blattel and Davidson, 2016; Kalfayan, 2008; Shafiq et al., 2014; Fink, 2015). As the concentrated acid moves down to the formation, it contacts with steel pipework and corrosion problems are inevitable. Management of these issues gulps a lot of funds and increases overall production cost. Therefore, corrosion inhibitors are introduced to the acidizing solution to delay or suppress dissolution and increase lifespan of associated steel materials (Fink, 2015).

Organic compounds that contain electron rich functionalities such as multiple bonds, oxygen, sulphur and nitrogen sites, heterocyclic and aromatic rings, have been used as corrosion inhibitors (Xhanari and Finšgar, 2016; Naveen et al., 2017; Yadav et al., 2016) but some of them are highly unfriendly, non-biodegradable and very expensive. Therefore, efforts have been made to develop metals corrosion inhibitors that are ecofriendly and affordable. However, some of the compounds reported in literature as ecofriendly inhibitors are only efficient at low temperatures and ineffective at high temperatures (Finšgar and Jackson, 2014), hence limiting their application in deep high temperature wells.

In this study, amitriptyline (AMI) was examined as base corrosion inhibitor for steel in oilfield pickling and acidizing environments. Three different grades of steel (X80, J55 and MS) commonly used in building well tubings were used. The pickling and acidizing environments were simulated using 3.7% and 15% HCl respectively and temperature was controlled between 30 °C and 90 °C. To boost the inhibitive strength of

* Corresponding author.
E-mail address: umoren@kfupm.edu.sa (S.A. Umoren).

https://doi.org/10.1016/j.petrol.2018.12.011
Received 10 August 2018; Received in revised form 30 November 2018; Accepted 4 December 2018
Available online 05 December 2018
0920-4105/

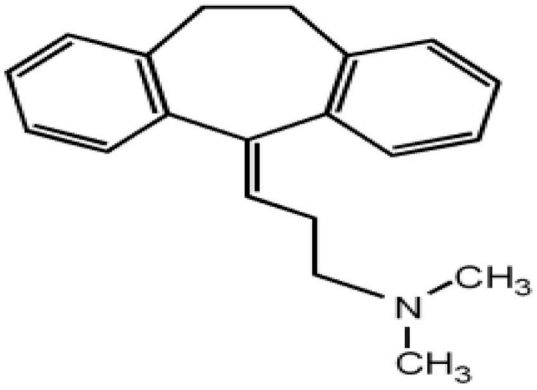

Fig. 1. Molecular structure of AMI.

AMI at simulated downhole temperatures, it was blended with some established synergistic compounds, namely potassium iodide, glutathione, and N-acetyl cysteine (Ituen et al., 2017). The choice of AMI was motivated by the presence of some of the electron-rich sites earlier mentioned in its molecular structure (see Fig. 1). In addition, AMI is not toxic and can be cheaply and renewably obtained from *Griffonia simplicifolia*, a shrub that grows abundantly in forests of southern Nigeria and many West African forests (Addotey, 2010).

The corrosion suppression performance of both the AMI and AMI-formulations was evaluated using weight loss, electrochemical impedance spectroscopy (EIS), and potentiodynamic polarization (PDP) techniques. The surfaces of some of the steel substrates were subjected to SEM-EDAX analyses while Fourier-transform infrared (FTIR) spectroscopic technique was used to elucidate the mechanism of corrosion inhibition.

2. Materials and methods

2.1. Metal specimens and surface preparation

Mild steel (MS) sheets were bought from the local Construction Materials Market in Uyo, Akwa Ibom State, Nigeria. The J55 and X80 steel grades were supplied by Qingdao Tengxiang Instrument and Equipment Co. Ltd., China. In Table 1 is listed the chemical compositions (Ituen et al., 2017) of the different steel grades. The metal sheets were cut into dimensions of 2 cm × 2 cm for gravimetric experiments, 1 cm × 1 cm for electrochemical measurements, and 2 cm × 1 cm for surface analysis examination. ASTM procedures were followed in preparing the steel surfaces (A. S. T. M. Standard, 2011) and in addition, the samples for electrochemical measurements were subjected to mechanical abrasion.

2.2. Test solutions

Typical pickling and acidizing environments were simulated by diluting analytical grade 37% HCl to 3.7% and 15% respectively using distilled water. The AMI (industrial grade, Meyers Co. Ltd., China) was utilized as supplied without further purification in the concentrations range of 1×10^{-5} to 10×10^{-5} M. The commercial inhibitor was supplied by Shell Nigeria.

2.3. Gravimetric measurements

Pre-weighed samples were immersed in the respective test solutions and their containers were placed in water bath maintained at 30 °C for 5 h. Thereafter, they were retrieved and cleaned using ASTM G31 standard procedures (A. S. T. M. Standard, 2011). Triplicates of such experiments were performed per test solution and repeated for other temperatures (45, 60, 75 and 90 °C). The weight losses ($m_o - m_1$) were recorded and the average value was used to compute the deterioration rate (CR) in mpy following Eq. (1). In where the corrosion rate values are presented in mm/yr, conversion was done as described in literature (Ahmad, 2006). The percentage corrosion retardation (ε_{WL}) and the extent of surface coverage (θ) respectively were computed making use of Eqs. (2) and (3).

$$CR(mpy) = \frac{3.45 \times 10^6 (m_0 - m_1)}{\rho A t} \quad (1)$$

Table 1
Composition of different grades of steel used.

Steel type	Chemical composition (wt. %)
MS	C (0.13), Si (0.18), Mn (0.39), P (0.40), S (0.04), Cu (0.025), Fe (balance)
J55	C (0.24), Si (0.22), Mn (1.1), P (0.103), S (0.004), Cu (0.5), Ni (0.28), Mo (0.019), Fe (balance)
X80	C (0.065), Si (0.24), Mn (1.58), P (0.011), S (0.003), Cu (0.01), Cr (0.022), Nb (0.057), V (0.005), Ti (0.024), B (0.0006), Fe (balance)

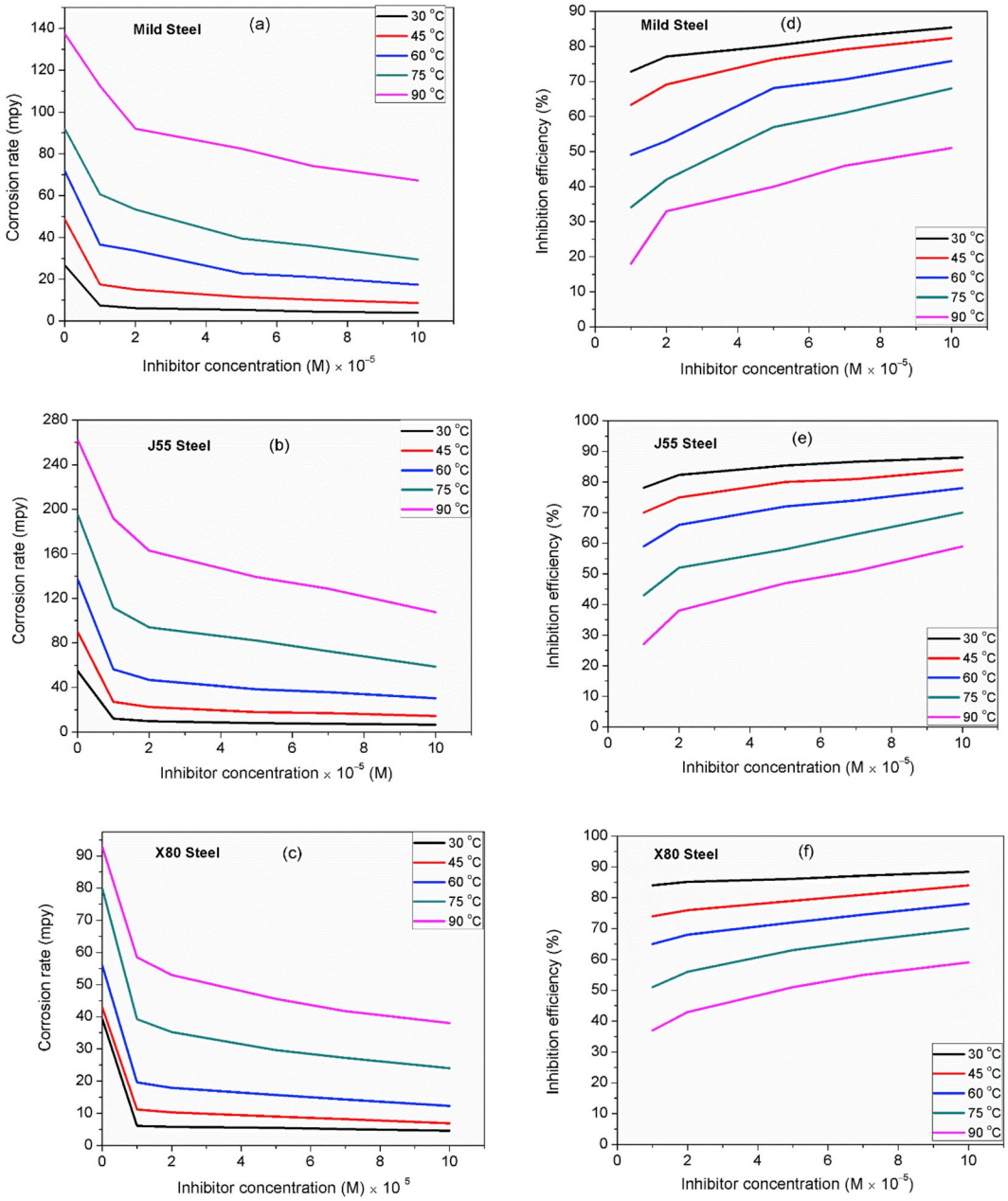

Fig. 2. Plot of (a–c) corrosion rate and (d–f) inhibition efficiency against inhibitor concentration in 3.7% HCl for the different steel types at different temperatures from weight loss measurements.

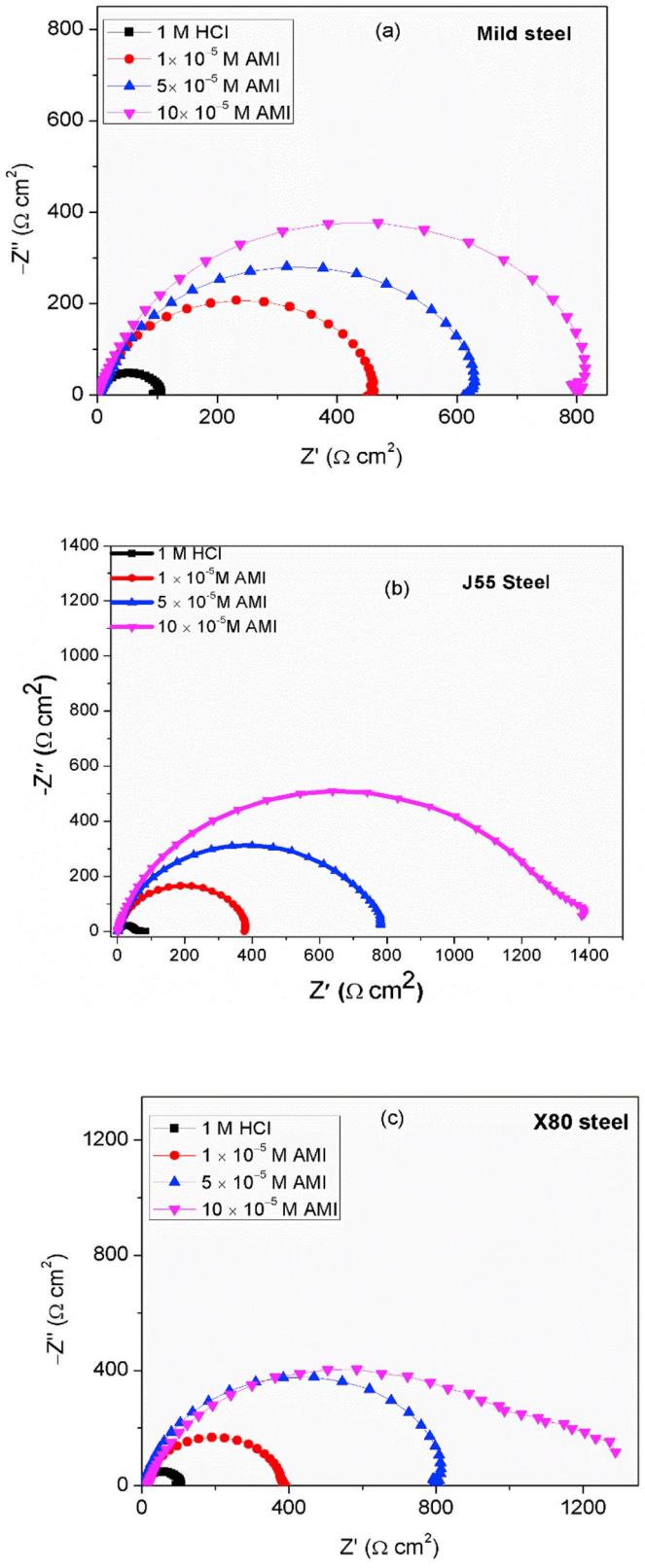

Fig. 3. Impedance plots for (a) mild steel, (b) J 55 steel, and (c) X80 steel in 3.7% HCl in the absence and presence of selected concentrations of AMI at 30 °C.

$$\varepsilon_{WL} = 100\left(\frac{CR_a - CR_i}{CR_a}\right) \quad (2)$$

$$\theta = 0.01\varepsilon_{WL} \quad (3)$$

where m_o and m_1 are the weights of the specimens before and after corrosion test, ρ is the density, A the surface area, CR_a and CR_i are the deterioration rates of steel in the free and fortified acid solutions.

2.4. Electrochemical monitoring techniques

Electrochemical tests were conducted for all the three steel grades in 3.7% HCl and selected concentrations of the inhibitor (1×10^{-5}, 5×10^{-5} and 10×10^{-5} M) only. Gamry ZRA (REF 600–18042) electrochemical workstation with tri-electrode set up (Pt mesh as counter electrode, saturated calomel electrode (SCE) as reference electrode, & steel specimen as working electrode) was utilized. Open circuit scan was run for 1800 s to achieve steady open circuit potential (OCP). EIS measurements were conducted utilizing frequency of 10^5 to 10^{-2} Hz at 30 °C. ASTM standard scan rate of 0.2 mV/s was adopted in PDP scanning from cathodic potential of −0.15 V vs. SCE to anodic potential of +0.15 V vs SCE relative to OCP. Data fittings and analyses were accomplished using Gamry E-Chem software package. Charge transfer resistance (R_{ct}) and corrosion current densities were used to calculate the inhibition efficiencies for EIS (ε_{EIS}) and PDP (ε_{EIS}) measurements according to Eq. (4) and Eq. (5) respectively.

$$\varepsilon_{EIS} = 100\left(\frac{R_{ctI} - R_{ctB}}{R_{ctI}}\right) \quad (4)$$

$$\varepsilon_{PDP} = 100\left(1 - \frac{I^i_{corr}}{I^b_{corr}}\right) \quad (5)$$

where R_{ctB} and R_{ctI} are measured charge transfer resistances in solution devoid of and with inhibitor respectively, and I^b_{corr} and I^i_{corr} are the measured corrosion current densities without and with inhibitor respectively. The magnitude of the double layer capacitance (C_{dl}) of the adsorbed film was evaluated from constant phase element (CPE) constant (Y_o) and R_{ct} via Eq. (6) (El Hamdani et al., 2015).

$$C_{dl} = (Y_0 R_{ct}^{n-1})^{1/n} \quad (6)$$

where n is a constant obtained from the phase angle given that $(j^2 = -1)\alpha$ and $n = 2\alpha/(\pi)$.

2.5. FTIR spectroscopy

This study was also conducted using MS in 3.7% HCl only. The FTIR chart of the as supplied AMI sample and that of the film extracted from the MS surface after immersion in studied systems were recorded.

2.6. SEM-EDAX study

The SEM images of the samples before and after immersion in 3.7% HCl for 5 h were recorded in vacuum mode. This was repeated with a sample immersed in HCl solution fortified with 10×10^{-5} M AMI. The instrument was accelerated at 5 kV. EDAX profiles of the surfaces were also obtained.

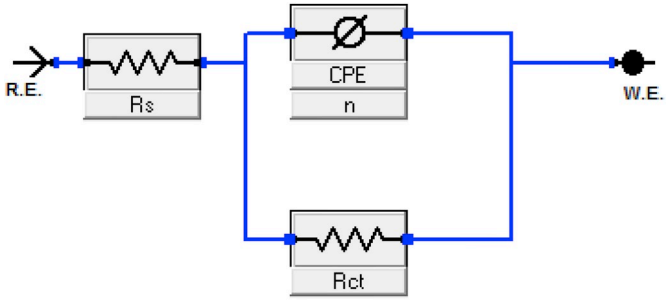

Fig. 4. Equivalent circuit used to analyze experimental data.

3. Results and discussion

3.1. Corrosion inhibition by AMI in 3.7% HCl

3.1.1. Gravimetric measurements

In Fig. 2(a–c) is shown the variation of corrosion rate of the different steel grades with AMI dose in 3.7% HCl solution at temperature ranging from 30 to 90 °C. As could be seen in the figure, in the blank acid solution, corrosion rate was highest with J55 steel and least with mild steel. Compared to acid solution devoid of AMI, presence of AMI causes a decrease in the corrosion rate but the influence of AMI is dose and temperature dependent. Worthy of note in Fig. 2(a–c) is the remarkable reduction of corrosion rate by all the concentrations of the inhibitor for the different substrates at 30 °C. In fact, the corrosion rate values ranged between 3 and 5 mpy in all cases. The industrial acceptable corrosion rate limit in inhibited environment is 4 mpy (0.1 mm/y) (Papir et al., 1989). AMI is therefore a promising corrosion inhibitor for pickling conditions. The protection efficiency increased with increasing AMI dose but decreased with rising temperature (Fig. 2(d–f)). The highest inhibition efficiency with the different steel grades was obtained with 10×10^{-5} M AMI concentration. The observed decrease in protection efficiency with rise in temperature is typical of a physisorption kind of adsorption (Solomon et al., 2010). Although AMI is most potent inhibitor for X80 steel corrosion (Fig. 2(f)), the inhibitor can be relied upon for other grades of steel but in pickling conditions (i.e 1 M HCl and 30 °C) since corrosion rate is within the acceptable industrial limit and the inhibition efficiency above 85%.

3.1.2. Electrochemical impedance spectroscopy (EIS)

Data obtained from the EIS study were used to construct Nyquist plots presented in Fig. 3. The graphs exhibit the characteristics of a typical charge transfer controlled corrosion process. For instance, each system is characterized by a single distorted capacitive loop with center under the real impedance axis (Banerjee et al., 2012). The distortion of the semicircles was caused by the heterogeneous nature of the working electrodes (Ehsani et al., 2017; Singh et al., 2017). The curves for all the tested solutions are however alike shape-wise showing that the dissolution mechanism is same notwithstanding the presence or absence of AMI (Solomon et al., 2017a). Nevertheless, depending on concentration, the presence of the additive effects the sizes of the semicircular curves signifying that addition of AMI delayed the deterioration rate of the steel. This may have been possible through the adsorption of AMI molecules onto the steel surface which covered corrosion active sites on the surface. The fitting of the Nyquist curves was done using a simple RQR equivalent circuit shown in Fig. 4 and the derived (R_s, R_{ct}, n, Y_0) and computed (C_{dl} and ε) electrochemical parameters are displayed in Table 2. The equivalent circuit gave a good fit as suggested by the chi square values (Table 2). The R_{ct} and C_{dl} as could be seen in Table 2 vary in opposite direction with AMI dose, i.e R_{ct} increases while C_{dl} decreases with increase in AMI dose. The observed trend is consistent with those reported by other researchers (James and Davies, 1976; Obi-Egbedi and Obot, 2013). The increase in R_{ct} and decrease in C_{dl} with increasing AMI dose may infer improved protection effect occasioned by the increase in the thickness of adsorbed additive layer. At the metal-solution interface, AMI protective layer is most likely to form. As AMI dose increases, the

Table 2
EIS parameters for the corrosion of MS, J55 and X80 steel in 3.7% HCl without and with selected concentrations of AMI at 30 °C.

Steel grade	AMI concentration (M)	R_s (Ω cm^2)	R_{ct} (Ω cm^2)	Y_o ($\mu\Omega^{-1}s^2cm^{-2}$)	n	C_{dl} (μFcm^{-2})	$\chi^2 \times 10^{-3}$	ε_{EIS}(%)
MS	Blank	1.035	102.3	582.7	0.872	7.06	0.72	–
	1×10^{-5}	1.182	462.4	291.9	0.849	1.53	0.12	77.9
	5×10^{-5}	1.196	623.6	130.8	0.874	0.96	0.84	83.6
	10×10^{-5}	1.243	835.5	105.9	0.870	0.70	0.09	87.8
J55	Blank	1.131	76.2	206.8	0.895	3.51	0.95	–
	1×10^{-5}	0.972	335.3	163.8	0.896	0.81	1.02	77.3
	5×10^{-5}	1.065	655.7	150.8	0.887	0.47	0.83	88.4
	10×10^{-5}	1.206	710.1	169.0	0.862	0.36	1.14	89.3
X80	Blank	1.063	79.6	352.3	0.812	6.60	1.03	–
	1×10^{-5}	1.005	379.8	146.9	0.821	0.33	0.78	79.0
	5×10^{-5}	1.210	786.8	126.4	0.845	0.05	0.19	89.9
	10×10^{-5}	1.224	1383.1	109.2	0.836	0.02	0.07	94.2

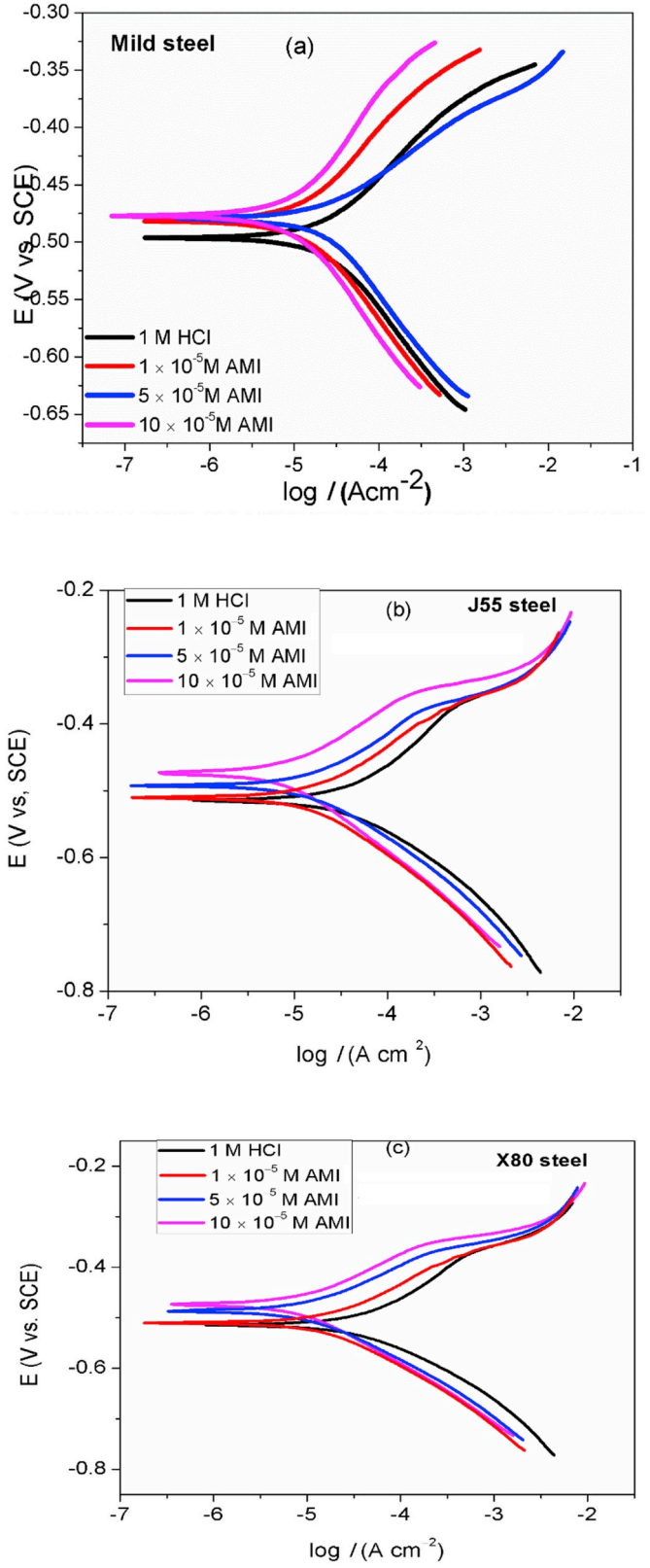

Fig. 5. Potentiodynamic polarization curves for the different steel types in 3.7% HCl in the absence and presence of selected concentrations of AMI at 30 °C.

adsorbed layer may have become thicker or multilayered. The interface between the solution and steel surface can also be considered to have bilayer of charges. One side of the layer may convey excess proton which may be balanced by excess electron on the other side of the layer, forming a kind of a capacitor as suggested by the values of the n parameter (the values of n in Table 2 is close to unity. For a pure capacitor, n = 1 (Solomon et al., 2017a)). It is also observed in Table 2 that n values are slightly higher (in many cases) in the protected systems than unprotected. This could mean that, the adsorption of the inhibitor species reduced the surface roughness of the electrode (Obi-Egbedi and Obot, 2013). Beside surface roughness, another possible reason could be corrosion rates and heterogeneous current distributions due to presence of adsorbed AMI film (Ituen et al., 2017). This observation justifies the introduction of a CPE in the equivalent circuit shown in Fig. 4 in place of a pure capacitor. The magnitudes of the protection efficiency of AMI obtained from this technique (Table 2) are comparable with those derived from gravimentric measurements (Fig. 2). The highest AMI concentration (10×10^{-5} M) afforded the best inhibition efficiency of 87.8%, 89.3%, and 94.2% for MS, J 55, and X80 respectively.

3.1.3. Potentiodynamic polarization measurements

Fig. 5 presents the potentiodynamic polarization curves for the different steel types in 3.7% HCl in the absence and presence of selected concentrations of AMI at 30 °C. The associated parameters namely, current densities (i_{corr}), anodic Tafel slope (β_a), cathodic slope (β_c), and corrosion potential (E_{corr}) deduced by extrapolation technique (Singh et al., 2017; Solomon et al., 2017a) are listed in Table 3. The E_{PDP} was calculated using Eq. (5). From Fig. 5, it is seen that both the anodic and cathodic current densities are reduced and E_{corr} slightly shifted in inhibited systems towards nobler direction relative to uninhibited. In Table 3, the E_{corr} values obtained on addition of AMI are more positive than that of the free acid solution. Also, the β_a values of the inhibited systems are remarkably bigger than those of the free acid solutions (Table 3) compared to β_c values. All these indicate that, although AMI may be said to function in the studied systems as a mixed type corrosion inhibitor, the effect on the anodic corrosion reactions was greater (Tao et al., 2012; Prabakaran et al., 2014). The efficiencies obtained from PDP method is in good agreement with those from EIS (Table 2) and gravimetric (Fig. 2) techniques.

3.2. Adsorption studies

Authors (Solomon et al., 2017a; Tao et al., 2012; Gerengi et al., 2016) have continued to use adsorption isotherm models in probing the adsorption mechanism of corrosion inhibitors on metals surfaces. This is because, vital information like the strength of interaction and mechanism of adsorption can be deduced from adsorption isotherm. There are several adsorption isotherm models; selection of the best model for a system is often done by making use of the linear regression coefficient (R^2) value. For an ideal situation, $R^2 = 1$. In our case, Langmuir adsorption isotherm was identified as the best model that describe the adsorption process of AMI onto the substrates surfaces. R^2 value in all cases was near unity (Table 4). The Langmuir isotherm model has the form (Solomon et al., 2017a):

$$\frac{C_{\text{inh}}}{\theta} = \frac{1}{K_{\text{ads}}} + C_{\text{inh}} \tag{7}$$

Table 3
Potentiodynamic polarization parameters for the corrosion of MS, J55 and X80 steel in 3.7% HCl without and with selected concentrations of AMI.

Steel Grade	AMI Conc. (M)	E_{corr}(mV/SCE)	i_{corr}(μA cm^{-2})	β_a(mV dec^{-1})	β_c(mV dec^{-1})	ε_{PDP}(%)
	Blank	−499	969.3	95.4	64.7	–
MS	1×10^{-5}	−480	210.3	106.2	71.6	78.3
	5×10^{-5}	−478	174.5	113.1	68.3	82.0
J55	10×10^{-5}	−476	114.4	121.9	73.2	94.4
X80	Blank	−473	619.4	71.3	101.2	–
	1×10^{-5}	−467	142.5	83.9	101.9	77.0
	5×10^{-5}	−464	78.0	94.2	97.2	87.4
	10×10^{-5}	−463	61.3	107.7	102.7	90.1
	Blank	−496	693.7	82.1	98.5	–
	1×10^{-5}	−482	149.8	96.0	87.4	78.4
	5×10^{-5}	−481	74.9	104.1	78.2	89.2
	10×10^{-5}	−474	44.4	133.6	84.8	93.6

where θ is the surface coverage and was derived from weight loss data using Eq. (3), K_{ads} is the equilibrium constant of the adsorption process, and C_{inh} is the concentration of AMI. Fig. 6 shows the linear graphs obtained by plotting C_{inh} against C_{inh} /θ for the various steel grades at temperature range of 30–90 °C. The K_{ads} values were derived from the intercepts of the graphs and were used in the calculation of the standard free energy (ΔG^0_{ads}) of the adsorption process according to the following equation (Solomon et al., 2017b):

$$\Delta G^0_{ads} = -RT \ln(55.5K_{ads}) \quad (8)$$

where R and T are the molar gas constant and absolute temperature respectively. From thermodynamic point of view, ΔG^0_{ads} would be related to the standard enthalpy (ΔH^0_{ads}) and entropy (ΔS^0_{ads}) of the adsorption process thus (Solomon et al., 2017a):

$$\Delta G^0_{ads} = \Delta H^0_{ads} + T\Delta S^0_{ads} \quad (9)$$

Combination and simplification of Eqs. (8) and (9) gives,

$$\ln K_{ads} = \frac{-\Delta H^0_{ads}}{RT} + \frac{\Delta S^0_{ads}}{R} - 4.016 \quad (10)$$

By plotting ln K_{ads} against $1/T$, linear graphs (Fig. 7) were obtained with ΔH^0_{ads} /R as the slope and ($\Delta S^0_{ads}/R$) − 4.016 as the intercept. All the parameters derived for the adsorption process of AMI on the substrates surfaces in 3.7% HCl are listed in Table 4. The K_{ads} values, as could be seen in the table are low and is a common feature of physical interaction (Solomon et al., 2017b; Zheng et al., 2015). The slopes of the Langmuir isotherm plots are more than

Table 4
Langmuir adsorption parameters for AMI in 3.7% HCl for different steel types at different temperatures.

Steel type	Temperature (°C)	ΔG^o_{ads} (kJ/mol)	K_{ads} (M^{-1})	Slope	R^2	ΔH^o_{ads} (kJ/mol)	ΔS^o_{ads} (J/mol/K)
Mild steel	30	−13.14	3.32	1.56	0.999	−39.89	−88.46
	45	−10.82	1.08	1.18	0.934		
	60	−10.79	0.89	1.22	0.996		
	75	−9.56	0.49	1.31	0.993		
	90	−8.28	0.28	1.63	0.987		
J55 steel	30	−14.13	4.91	1.12	0.999	−42.33	−91.02
	45	−13.47	2.94	1.17	0.999		
	60	−12.68	1.76	1.24	0.998		
	75	−10.86	0.77	1.35	0.989		
	90	−9.36	0.40	1.51	0.985		
X80 steel	30	−16.03	10.46	1.13	0.999	−46.18	−100.22
	45	−13.88	3.43	1.18	0.999		
	60	−12.22	1.23	1.20	0.988		
	75	−11.38	1.10	1.37	0.997		
	90	−11.00	0.69	1.58	0.996		

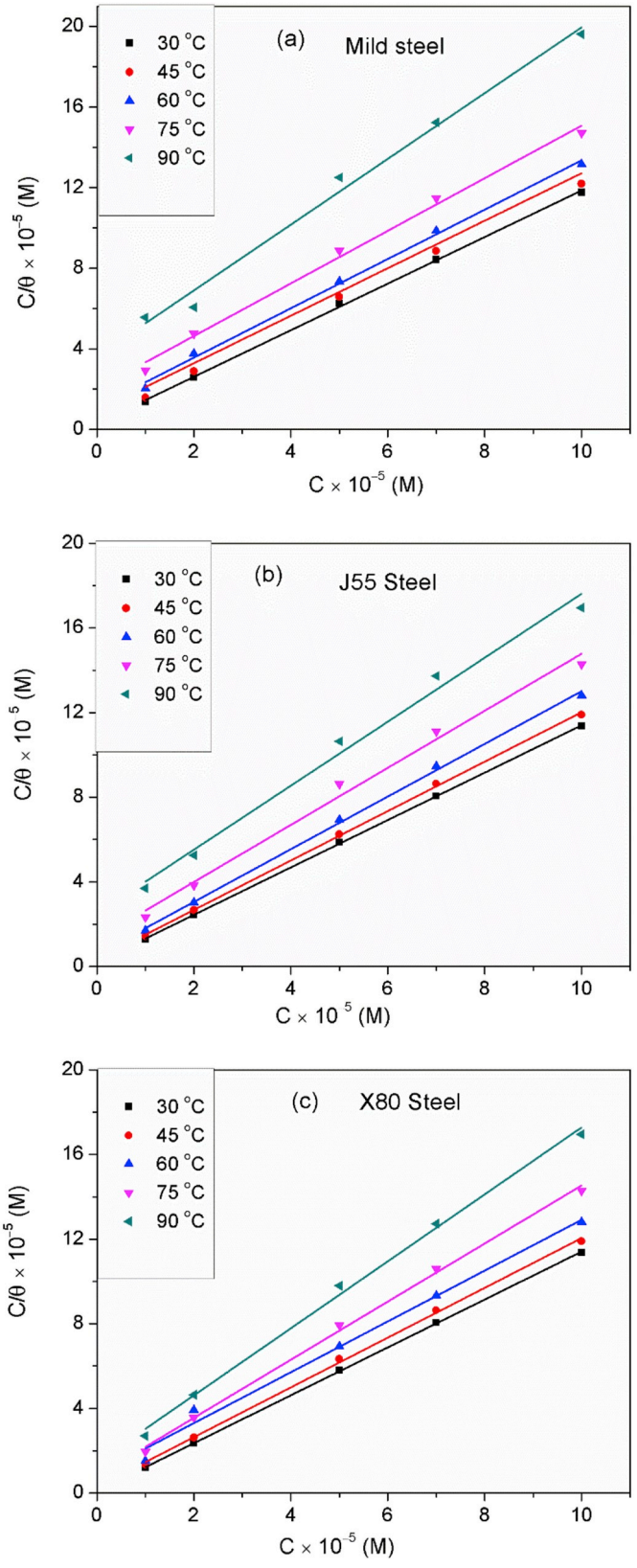

Fig. 6. Langmuir adsorption isotherm for AMI on (a) mild steel, (b) J55 steel and (c) X80 steel in 3.7% HCl at different temperatures.

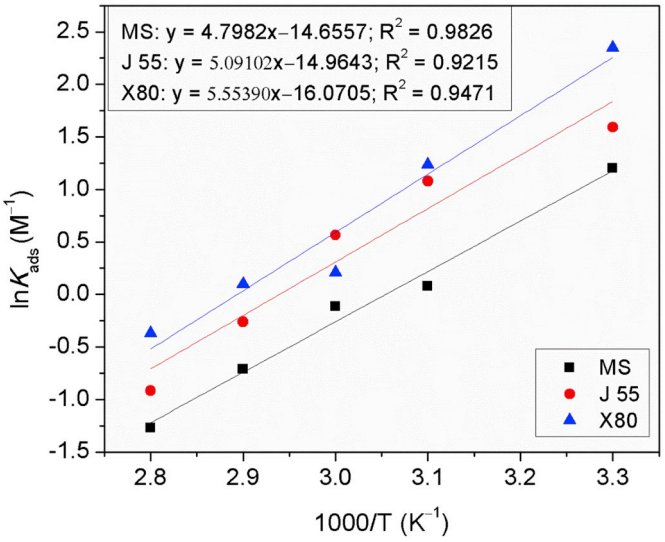

Fig. 7. The plot of $\ln K_{ads}$ vs T for the adsorption of AMI on mild steel, J55 steel and X80 steel in 3.7% HCl.

unity required by an ideal Langmuir isotherm model. This points to possible multiple layer formation by adsorbed species and also interaction between adsorbed species. During the derivation of Langmuir equation, these parameters were erroneously omitted (Solomon et al., 2010). The calculated ΔG^0_{ads} values are negative and this signifies the spontaneity of the adsorption process as well as the stability of the adsorbed inhibitor film (Badiea and Mohana, 2009). Generally, positive value of ΔH^0_{ads} means endothermic process while negative value implies exothermic process (Solomon et al., 2017a). In an endothermic adsorption process, $\Delta H^0_{ads} > 0$ infers chemical adsorption while $\Delta H^0_{ads} < 0$ indicates physical adsorption (Solomon et al., 2017a; Hoseinzadeh et al., 2014). In the same vain, in exothermic process, $\Delta H^0_{ads} < 40$ kJ/mol signifies physical adsorption while ΔH^0_{ads} value near 100 kJ/mol points to chemical adsorption (Solomon et al., 2017a; Tao et al., 2012). In our case, the ΔH^0_{ads} is negative meaning exothermic adsorption process. The magnitude of the ΔH^0_{ads} value is rather approximately equal to 40 kJ/mol in the case of MS and greater than 40 kJ/mol for J 55 and X80 substrates. This can be interpreted as mixed adsorption type (i.e both physical and chemical adsorption mechanisms) but with physical adsorption mechanism being the dominant. Similar interpretation had been given by Tao et al. (2012). The ΔS^0_{ads} values are negative and could be associated with the decrease in the degree of perturbation of the AMI inhibited systems on moving from reactants to the substrates adsorbed species (Solomon et al., 2017a; Tao et al., 2012).

3.3. Corrosion kinetics consideration

In real field situation, as temperature increases down a bore-hole, the performance of the inhibitor may decline due to thermal decomposition. Informed by this, the contribution of temperature to the corrosion of the different steel grades in 3.7% HCl without and with AMI was investigated at 30–90 °C. The results presented graphically in Fig. 2 clearly shows that temperature had a remarkable effect on the corrosion process. The relationship between corrosion rate and temperature can be visualized in the Arrhenius equation (Eq. (11)) (Solomon et al., 2017b), i.e the logarithm of corrosion rate varies linearly with $1/T$.

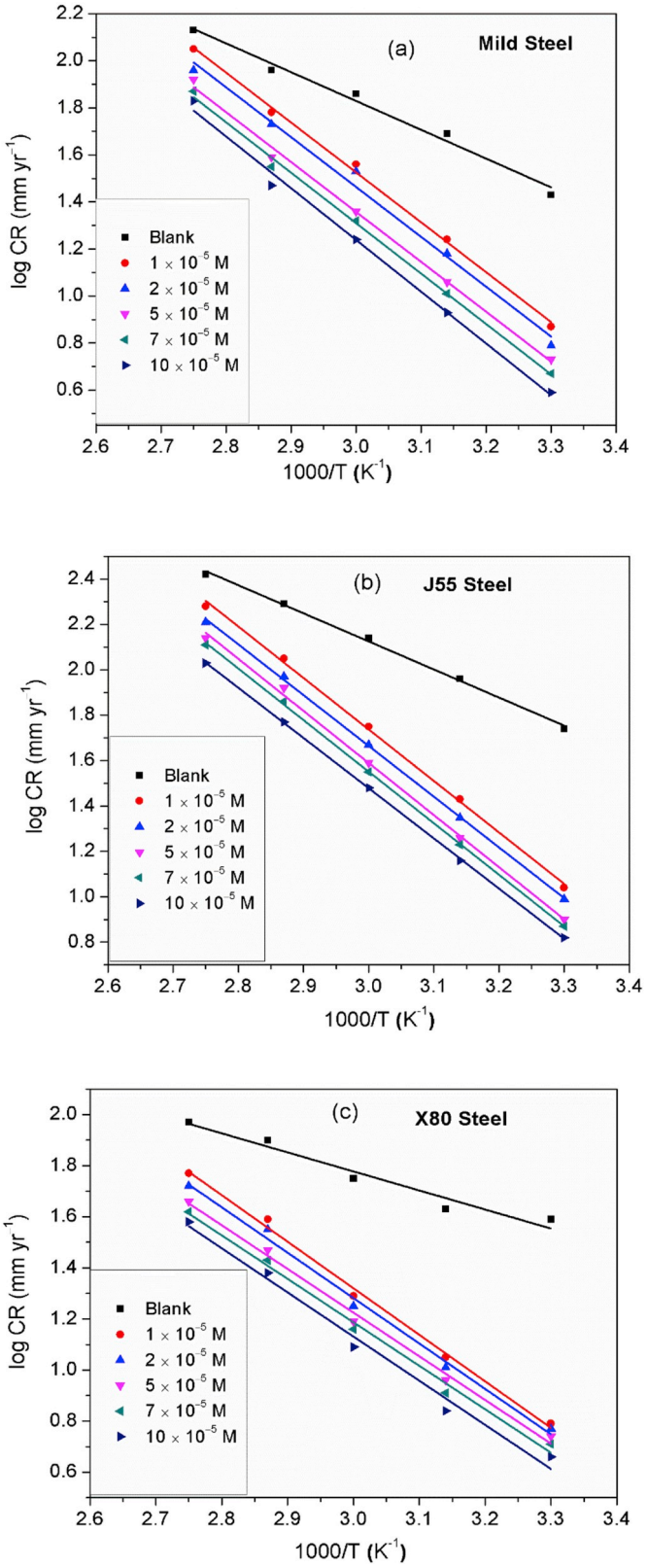

Fig. 8. Arrhenius plot of Log CR versus 1/T for (a) mild steel, (b) J55 steel and (c) X80 steel in 3.7% HCl in the absence and presence of different concentrations of AMI.

Table 5
Kinetic/thermodynamic parameters for steel types in 3.7% HCl without and with different concentrations of AMI.

Steel type	Concentration (M) × 10^{-5}	E_a (kJ/mol)	ΔH^* (kJ/mol)	ΔS^* (J/mol/K)
Mild steel	Blank	23.44	21.04	−147.75
	1	40.61	37.82	−103.19
	2	40.57	38.18	−103.28
	5	40.59	37.96	−105.95
	7	41.05	38.57	−105.08
	10	42.11	39.33	−104.17
J55 steel	Blank	23.68	20.44	−143.82
	1	43.41	39.46	−94.09
	2	42.80	40.01	−93.94
	5	43.92	41.11	−92.21
	7	43.48	40.69	−94.08
	10	42.34	39.35	−98.89
X80 steel	Blank	14.28	11.49	−177.37
	1	34.89	32.10	−124.28
	2	34.04	31.54	−126.73
	5	32.74	30.08	−132.20
	7	32.59	30.08	−132.97
	10	33.09	30.30	−133.29

$$\mathrm{Log}CR = \log A - \left(\frac{E_a}{2.303RT}\right) \tag{11}$$

where CR is the deterioration rate, E_a is the activation energy, and A is the frequency factor. Fig. 8 depicts the Arrhenius plots of log CR versus $1/T$ obtained for the different steel grades in the studied environment. The slope of the graphs is $-E_a/2.303R$ from which the E_a values were calculated from and listed in Table 5. It is seen in the table that the E_a values of the AMI inhibited acid solutions are bigger than those of uninhibited solutions. This means that, AMI inhibited the steel corrosion by raising the energy barrier of the corrosion reactions (Tao et al., 2012). According to authors (Tao et al., 2012; Solomon et al., 2017a, b), such behavior is common when the mechanism of adsorption is physisorption.

Alternatively, Arrhenius equation can be written in the form given in Eq. (12) (the so-called Transition State equation) (Solomon et al., 2017b):

$$\log\left(\frac{CR}{T}\right) = \left[\left(\log\left(\frac{R}{Nh}\right) + \left(\frac{\Delta S^*}{2.303R}\right)\right)\right] - \frac{\Delta H^*}{2.303RT} \tag{12}$$

where ΔH^* = the activation enthalpy, ΔS^* = the entropy of activation, N = Avogadro's number, and h = Planck's constant. Fig. 9 presents the graphs of log (CR/T) versus $1/T$ drawn for the studied systems. The ΔH^* and ΔS^* values which are listed in Table 5 were computed from the slopes ($-\Delta H^*/2.303R$) and intercepts ((log (R/Nh) + ($\Delta S^*/2.303R$)) of the graphs respectively. The ΔH^* values are positive and this portrays an endothermic nature of the activated step of the corrosion process (El-Taib Heakal et al., 2018). Furthermore, the ΔH^* values of inhibited systems are bigger compared to uninhibited and infers a slower corrosion rate in the inhibited systems (Yadav et al., 2012; El-Taib Heakal et al., 2011). The ΔS^* values are seen to be negative and large and is indicative of the fact that the activated complex in the rate determining step stands for an association instead of a dissociation [20, 26, 30]. Again, the ΔS^* values of inhibited acid solutions are more positive than those of uninhibited. According to El-Taib Heakal et al. (2018), this observation could be caused by the increase in solvent entropy due to water desorption from substrate surface in the presence of inhibitor.

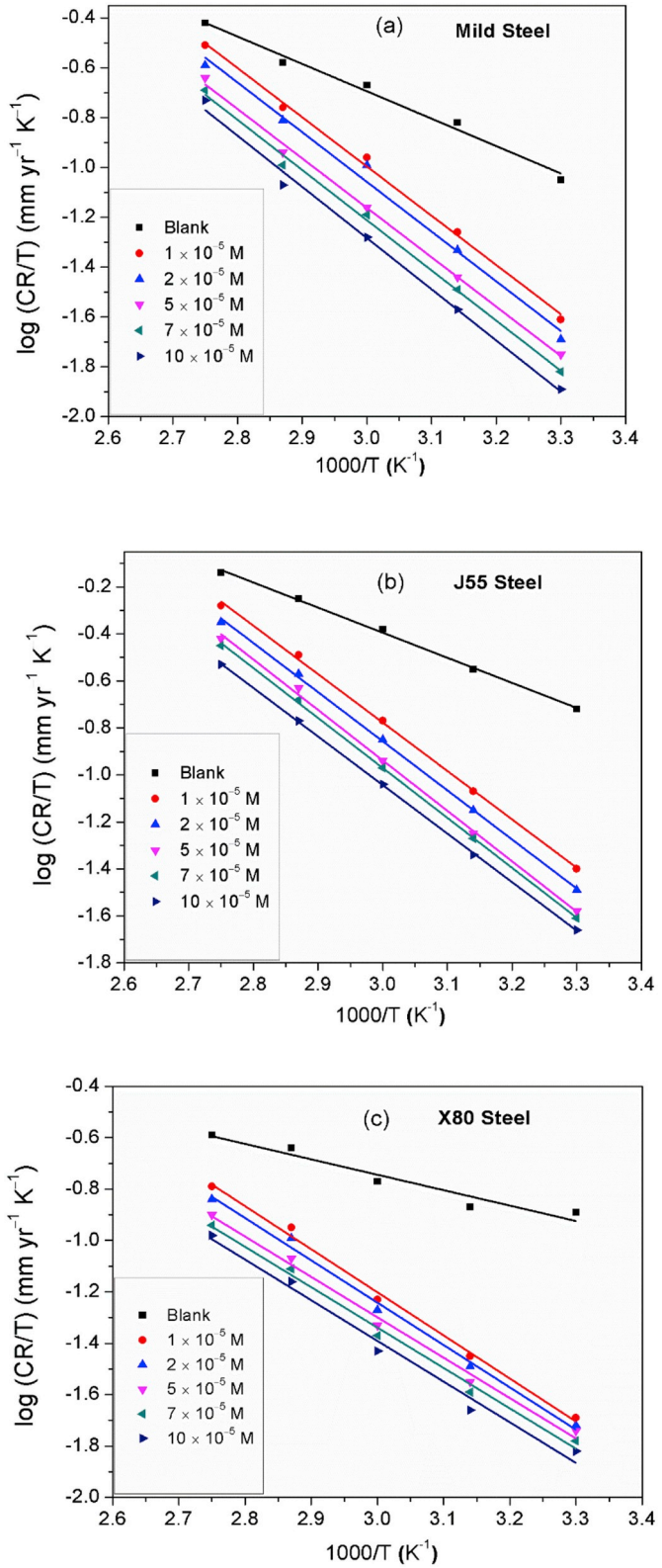

Fig. 9. Transition state plot of Log (CR/T) versus 1/T for (a) mild steel, (b) J55 steel and (c) X80 steel in 3.7% HCl in the absence and presence of different concentrations of AMI.

3.4. Corrosion inhibition by AMI based formulations in 3.7% and 15% HCl

The results (Fig. 2, Tables 2 and 3) obtained in this investigation portray AMI as promising inhibitor for steel in HCl medium. We however deem it important to compare the performance of highest studied concentration (10×10^{-5} M) of AMI with that of a commercial inhibitor at different experimental conditions. The deterioration rate and protection efficiency values obtained from the study are presented in Table 6. As could be seen in the table, the AMI performance is far below that of the commercial inhibitor at high temperatures. For instance, at 90 °C, the corrosion inhibition efficiency of AMI in 3.7% and 15% HCl media is 59% and 09% whereas the same concentration of commercial inhibitor has corrosion inhibition efficiency of 100% and 94% respectively. This finding was not surprising knowing that commercial inhibitors are multi-component formulations. The finding however prompted us to develop various AMI based formulations and examined their anticorrosive properties under the same conditions as the commercial inhibitor. In Table 7 is presented the composition of the formulations which are designated as AC1, AC2, AC3, and AC4. The results obtained for the formulations are also listed in Table 6. As could be clearly seen in Table 6, the AMI based formulations particularly AC2 and AC4 compete favorably with the commercial inhibitor. It is interesting to note that the AC4 formulation retain its corrosion inhibition effectiveness even in severe conditions. For instance, in 15% HCl solution at 90 °C, the inhibition efficiency of AC4 is 92% while that of the commercial inhibitor is 94%. The improved inhibition efficacy of the formulations can be attributed to synergism between the components (Finšgar and Jackson, 2014).

3.5. Surface analysis

The surface of MS immersed in 3.7% HCl without and with AMI was scanned by SEM-EDAX and the profiles obtained are given in Fig. 10. The surface of MS in the acid without the inhibitor was greatly damaged (Fig. 10(a)) whereas the surface was protected in the presence of the inhibitor (Fig. 10(c)). A thin film of adsorbed AMI is visible in the presence of AMI (Fig. 10(c)) which indicates that AMI inhibits steel corrosion by adsorption. Some parts of the surfaces scanned by EDAX (Fig. 10(d)) reveals the presence of chloride ions in the film which could have resulted from bridge-like formation between the metal surface and adsorbed AMI species. These chloride ions may have replenished charged steel surface allowing protonated AMI species to be electrostatically drag onto the surface (Ituen et al., 2017). In order to predict the functionality (ies) in AMI that participated in the adsorption process, the FTIR spectrum of pure AMI and that of film extracted from the metal surface was compared (see Fig. 11). The chart of pure AMI shows the characteristic bands of C—N stretching of the $(CH_3)_2$—N—CH_2— group at 1450 -1490 cm^{-1} (Socrates, 1980) and the aromatic vibration signals at 900 -1100 cm^{-1}. These peaks have been remarkably altered in the extracted film spectrum. These peaks seem to disappear in the extracted film spectrum. This suggests that these functionalities may have been used to interact with the steel surface during adsorption.

4. Conclusion

On the basis of results obtained from the assessment of amitriptyline (AMI) and its formulations as corrosion inhibitor for X80, J55 and mild steel (MS) in both 3.7% and 15% HCl, the following conclusions are drawn:

Table 6
Corrosion rate and inhibition efficiency for different steel grades in 3.7% and 15% HCl solutions without and with 10×10^{-5} M AMI alone and in combination with different formulations at different temperatures.

Steel grade		Mild steel						J 55 steel						X80 steel					
Medium	Inhibitor	CR (mm/yr)			ε (%)			CR (mm/yr)			ε (%)			CR (mm/yr)			ε (%)		
		30 °C	60 °C	90 °C	30 °C	60 °C	90 °C	30 °C	60 °C	90 °C	30 °C	60 °C	90 °C	30 °C	60 °C	90 °C	30 °C	60 °C	90 °C
3.7% HCl	Blank	26.72	71.82	137.36	–	–	–	54.87	137.41	262.60	–	–	–	39.45	56.11	92.92	–	–	–
	AMI	3.90	17.34	67.31	85	76	51	6.58	30.23	107.67	88	60	30	4.57	12.34	38.09	88	78	59
	AC1	2.39	10.91	49.17	91	85	64	31.82	31.05	106.61	94	77	59	2.13	7.29	26.02	95	87	72
	AC2	0.26	2.08	13.32	99	97	90	0.71	8.66	29.15	99	94	89	0.47	1.12	8.27	99	98	91
	AC3	1.05	9.19	26.24	96	87	81	1.87	20.47	64.34	97	85	76	0.75	5.61	14.68	98	90	84
	AC4	0.02	0.07	5.08	100	100	96	0.27	1.92	14.44	100	99	95	0.08	0.11	4.09	100	100	96
	Commercial inhibitor	0.01	0.03	0.06	100	100	100	0.05	0.27	2.11	100	100	99	0.00	0.06	0.279	100	100	100
15% HCl	Blank	153.94	209.30	338.66	–	–	–	161.02	195.81	294.19	–	–	–	155.03	215.80	342.04	–	–	–
	AMI	68.16	136.05	338.66	56	35	–	80.33	154.69	294.19	44	21	0	61.88	120.85	338.96	60	44	09
	AC1	28.94	62.79	192.32	81	70	43	32.20	66.38	185.34	80	66	37	26.20	61.93	164.18	83	71	52
	AC2	12.62	37.05	106.80	92	82	68	8.05	42.29	105.61	95	78	64	4.96	27.19	98.85	97	87	71
	AC3	36.48	88.12	223.76	76	58	34	47.98	95.75	210.64	70	51	28	35.35	81.37	177.18	77	62	48
	AC4	1.85	8.37	29.74	99	96	91	2.89	9.01	32.07	98	95	89	1.40	9.71	28.73	99	96	92
	Commercial inhibitor	0.60	3.56	23.32	100	98	93	0.64	5.29	23.83	100	97	92	0.47	4.75	21.21	100	98	94

Table 7
Compositions of the different AMI based corrosion inhibitor formulations.

Composite	Composition
AC1	10×10^{-5} AMI + 0.01 M potassium iodide (KI)
AC2	10×10^{-5} AMI + 1×10^{-5} M glutathione (GLT)
AC3	10×10^{-5} AMI + 1×10^{-5} M N-acetyl cysteine (NAC)
AC4	10×10^{-5} AMI + 0.01 M KI + 1×10^{-5} M GLT + 1×10^{-5} M NAC

- AMI is more efficient as corrosion inhibitor for all the studied steel grades in 3.7% HCl than 15% HCl.
- Inhibition efficiency of AMI and its formulations decrease with rise in temperature.
- Inhibitive effect of AMI is by formation of adsorbed film visible with SEM.
- Adsorption of AMI is associated with nitrogen and aromatic sites present in its molecular structure.
- The formulations of AMI are efficient at 90 °C, especially AC4 due to synergistic effect of the additives.
- AC4 can be employed as efficient corrosion inhibitor in oil and gas production

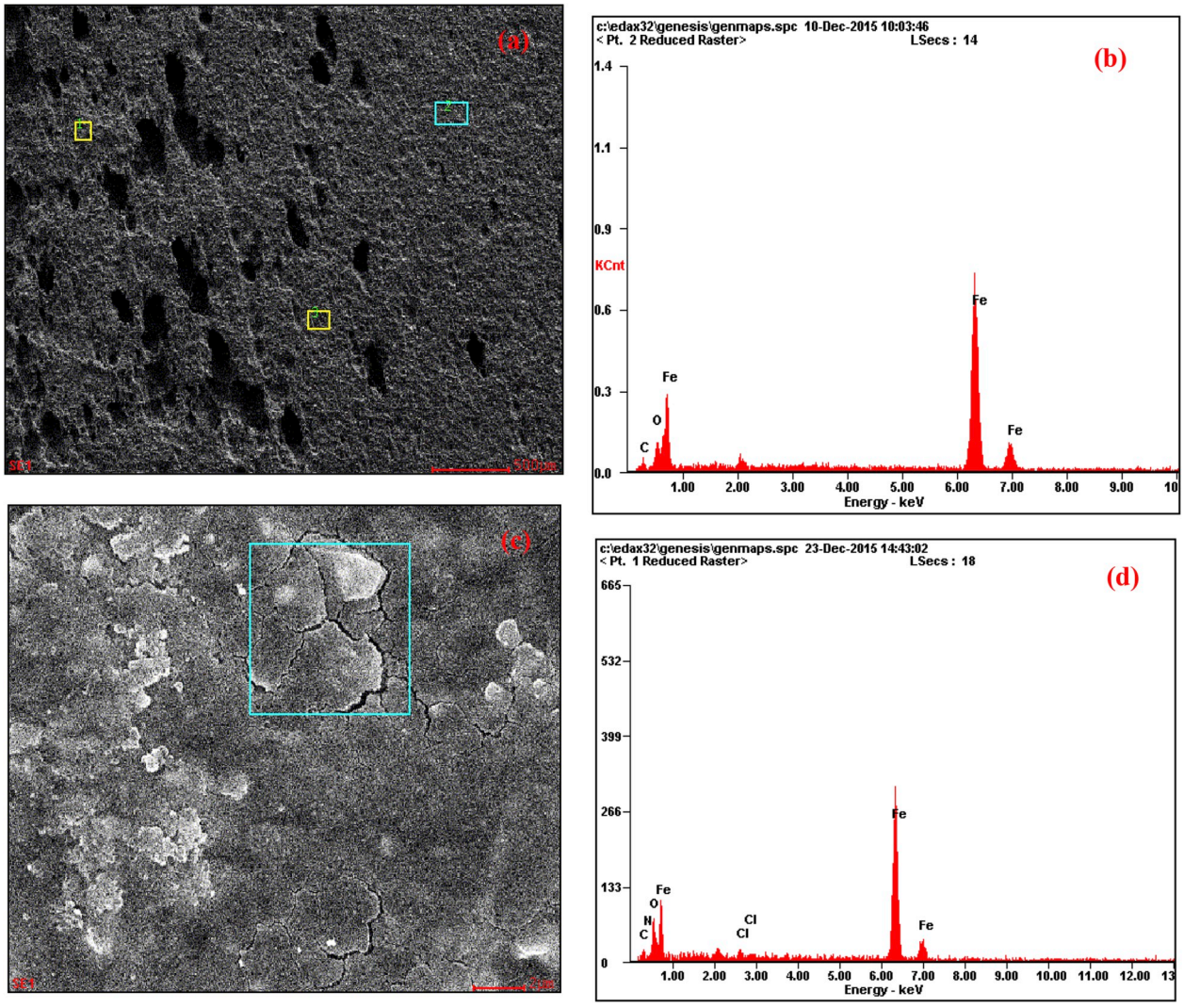

Fig. 10. SEM-EDAX profiles of MS in the (a, b) uninhibited and (c, d) AMI inhibited 3.7% HCl solution.

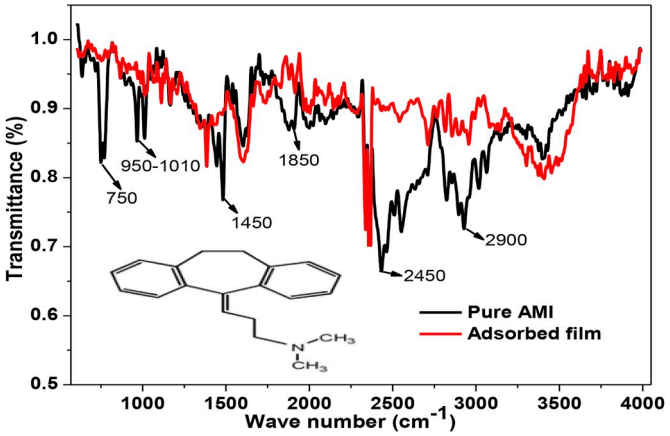

Fig. 11. FTIR spectra of pure AMI and AMI surface film on mild steel after corrosion in 3.7% HCl containing 10×10^{-5} M AMI.

Statement on conflict of interest

No conflict of interest exists with this manuscript.

Acknowledgements

The authors are grateful to Dr. Shuangqing Sun of Corrosion Protection Group, Department of Materials Physics and Chemistry, China University of Petroleum, Qingdao for providing the facilities and software for this work. Dr. Ituen gratefully acknowledged the support from World Bank under the World Bank RSM fellowship.

References

Addotey, A., 2010. Local Production of 5-HTP from the Seeds of *Griffonia simplicifolia*. Doctoral dissertation. Kwame Nkrumah University of Science and Technology, Kumasi, Ghana. http://hdl.handle.net/123456789/92.

Ahmad, Z., 2006. Principles of Corrosion Engineering and Corrosion Control. Butterworth-Heinemann.

Badiea, A.M., Mohana, K.N., 2009. Effect of temperature and fluid velocity on corrosion mechanism of low carbon steel in presence of 2-hydrazino-4,7-dimethylbenzothiazole in industrial water medium. Corrosion Sci. 51, 2231–2241. https://doi.org/10.1016/j.corsci.2009.06.011.

Banerjee, S., Srivastava, V., Singh, M.M., 2012. Chemically modified natural polysaccharide as green corrosion inhibitor for mild steel in acidic medium. Corrosion Sci. 59, 35–41. https://doi.org/10.1016/j.corsci.2012.02.009.

Blattel, S., Davidson, E., 2016. Method of Stimulating a Subterranean Formation Using an Acid Precursor Composition. US Patent WO2016108877A1.

Ehsani, A., Mahjani, M.G., Hosseini, M., Safari, R., Moshrefi, R., Mohammad, S.H., 2017. Evaluation of *Thymus vulgaris* plant extract as an eco-friendly corrosion inhibitor for stainless steel 304 in acidic solution by means of electrochemical impedance spectroscopy, electrochemical noise analysis and density functional theory. J. Colloid Interface Sci. 490, 444–451. https://doi.org/10.1016/j.jcis.2016.11.048.

El Hamdani, N., Fdil, R., Tourabi, M., Jama, C., Bentiss, F., 2015. Alkaloids extract of *Retama monosperma* (L.) Boiss. seeds used as novel eco-friendly inhibitor for carbon steel corrosion in 1M HCl solution: electrochemical and surface studies. Appl. Surf. Sci. 357, 1294–1305. https://doi.org/10.1016/j.apsusc.2015.09.159.

El-Taib Heakal, F., Fouda, A.S., Radwan, M.S., 2011. Inhibitive effect of some thiadiazole derivatives on C-steel corrosion in neutral sodium chloride solution. Mater. Chem. Phys. 125, 26–36. https://doi.org/10.1016/j.matchemphys.2010.08.067.

El-Taib Heakal, F., Deyab, M.A., Osman, M.M., Elkholy, A.E., 2018. Performance of *Centaurea cyanus* aqueous extract towards corrosion mitigation of carbon steel in saline formation water. Desalination 425, 111–122. https://doi.org/10.1016/j.desal.2017.10.019.

Fink, J., 2015. Petroleum Engineer's Guide to Oil Field Chemicals and Fluids. Gulf Professional Publishing, Amsterdam.

Finšgar, M., Jackson, J., 2014. Application of corrosion inhibitors for steels in acidic media for the oil and gas industry: a review. Corrosion Sci. 86, 17–41. https://doi.org/10.1016/j.corsci.2014.04.044.

Gandossi, L., 2013. An Overview of Hydraulic Fracturing and Other Formation Stimulation Technologies for Shale Gas Production. European Commisison Joint Research Centre Technical Reports. https://doi:10.2790/99937.

Gerengi, H., Mielniczek, M., Gece, G., Solomon, M.M., 2016. Experimental and quantum chemical evaluation of 8-hydroxyquinoline as a corrosion inhibitor for copper in 0.1 M HCl. Ind. Eng. Chem. Res. 55, 9614–9624. https://pubs.acs.org/doi/abs/10.1021/acs.iecr.6b02414.

Hoseinzadeh, A.R., Danaee, I., Maddahy, M.H., Avei, M.R., 2014. Taurıne as a green corrosıon inhıbıtor for AISI 4130 steel alloy in hydrochlorıc acid solutıon. Chem. Eng. Commun. 201, 380–402. https://doi.org/10.1080/00986445.2013.773425.

Ituen, E.B., Akaranta, O., Umoren, S.A., 2017. N-acetyl cysteine based corrosion inhibitor formulations for steel protection in 15% HCl solution. J. Mol. Liq. 246, 112–118. https://doi.org/10.1016/j.molliq.2017.09.040.

James, A.M., Davies, C.W., 1976. Dictionary of Electrochemistry. Palgrave Macmillan, United Kingdom. https://doi.10.1007/978-1-349-02820-7.

Kalfayan, L., 2008. Production Enhancement with Acid Stimulation. Pennwell Books, Tusla, Okla.

Naveen, E., Ramnath, B.V., Elanchezhian, C., Nazirudeen, S.M., 2017. Influence of organic corrosion inhibitors on pickling corrosion behaviour of sinter-forged C45 steel and 2% Cu alloyed C45 steel. J. Alloy. Comp. 695, 3299–3309. https://doi.org/10.1016/j.jallcom.2016.11.133.

Obi-Egbedi, N.O., Obot, I.B., 2013. Xanthione: a new and effective corrosion inhibitor for mild steel in sulphuric acid solution. Arabian J. Chem. 6, 211–223. https://doi.org/10.1016/j.arabjc.2010.10.004.

Papir, Y.S., Schroeder, A.H., Stone, P.J., 1989. New downhole filming amine corrosion inhibitor for sweet and sour production. In: SPE 18489 Presented at the SPE International Symposium on Oilfield Chemistry in Houston, TX, February 8-10. https://doi.org/10.2118/18489-MS.

Prabakaran, M., Vadivu, K., Ramesh, S., Periasamy, V., 2014. Corrosion protection of mild steel by a new phosphonate inhibitor system in aqueous solution. Egyptian J. Pet. 23 (4), 367–377. https://doi.org/10.1016/j.ejpe.2014.09.004.

Shafiq, M.U., Shuker, M.T., Kyaw, A., 2014. Performance comparison of new combinations of acids with mud acid in sandstone acidizing. Res. J. Appl. Sci. Eng. Technol. 7 (2), 323–328. https://doi:10.19026/rjaset.7.258.

Singh, A., Ansari, K.R., Kumar, A., Liu, W., Songsong, C., Lin, Y., 2017. Electrochemical, surface and quantum chemical studies of novel imidazole derivatives as corrosion inhibitors for J55 steel in sweet corrosive environment. J. Alloy. Comp. 712, 121–133. https://doi.org/10.1016/j.jallcom.2017.04.072.

Socrates, G., 1980. Infrared Characteristic Group Frequencies. John Wiley & Sons, NewYork, pp. 54.

Solomon, M.M., Umoren, S.A., Udosoro, I.I., Udoh, A.P., 2010. Inhibitive and adsorption behaviour of carboxymethyl cellulose on mild steel corrosion in sulphuric acid solution. Corrosion Sci. 52, 1317–1325. https://doi.org/10.1016/j.corsci.2009.11.041.

Solomon, M.M., Gerengi, H., Umoren, S.A., 2017a. Carboxymethyl cellulose/silver nanoparticles composite: synthesis, characterization and application as a benign corrosion inhibitor for St37 steel in 15% H_2SO_4 medium. ACS Appl. Mater. Interfaces 9, 6376–6389. https://pubs.acs.org/doi/abs/10.1021/acsami.6b14153.

Solomon, M.M., Gerengi, H., Kaya, T., Kaya, E., Umoren, S.A., 2017b. Synergistic inhibition of St37 steel corrosion in 15% H_2SO_4 solution by chitosan and iodide ion additives. Cellulose 24, 931–950. https://doi.10.1007/s10570-010-9409-7.

Standard, A.S.T.M., 2011. G1-03 Standard Practice for Preparing, Cleaning and Evaluating Corrosion Test Specimens.

Tao, Z., He, W., Wang, S., Zhang, S., Zhou, G., 2012. A study of differential polarization curves and thermodynamic properties for mild steel in acidic solution with nitrophenyltriazole derivative. Corrosion Sci. 60, 205–213. https://doi.org/10.1016/j.corsci.2012.03.035.

Xhanari, K., Finšgar, M., 2016. Organic corrosion inhibitors for aluminum and its alloys in chloride and alkaline solutions: a review. Arabian J. Chem. https://doi.org/10.1016/j.arabjc.2016.08.009.

Yadav, D.K., Quraishi, M., Maiti, B., 2012. Inhibition effect of some benzylidenes on mild steel in 1 M HCl: an experimental and theoretical correlation. Corrosion Sci. 55, 254–266. https://doi.org/10.1016/j.corsci.2011.10.030.

Yadav, M., Behera, D., Sharma, U., 2016. Nontoxic corrosion inhibitors for N80 steel in hydrochloric acid. Arabian J. Chem. 9 (2), S1487–S1495. https://doi.org/10.1016/j.arabjc.2012.03.011.

Zheng, X., Zhang, S., Li, W., Gong, M., Yin, L., 2015. Experimental and theoretical studies of two imidazolium-based ionic liquids as inhibitors for mild steel in sulfuric acid solution. Corrosion Sci. 95, 168–179. https://doi.org/10.1016/j.corsci.2015.03.012.